Journal of the Korean Association of Crystal Growth
Vol. 10, No. 5 (2000) 356-361

Comparison of numerical simulation and experiment for the OiSF-Ring diameter in czochralski-grown silicon crystal

Hyun Jung Oh, Jong Hoe Wang and Hak-Do Yoo
R&D Center, LG Siltron Inc., Kumi 730-350, Korea
(Received April 21, 2000)

Abstract The radial position of OiSF-ring has been meaningful data in industry. Thus it's position was calculated by application of $(V/G)_{crit} = 0.138\ mm^2/minK$ and point defect dynamics for industrial scale grower with various pull rates. After the calculation, compared with experimental result. OiSF-ring diameters expected with calculation were good agreement with experimental results. In order to show validity of the predicted temperature distribution using STHAMAS which is one of the global simulator for Cz crystal growing, temperature was measured along the axis of crystal using thermocouples, and compared with the calculated temperature. We found the effective thermal conductivity K_m (r) which gives in accordance with the temperature distribution at the axis of crystal and crystal/melt interface shape between experimental and computational results. Therefore, effective thermal conductivity K_m (r) was applied instead of solving melt convection problem.

1. Introduction

Oxidation Induced Staking Faults (OiSFs) which appear in a ring pattern distribution have been considered as very urgent problem for many years. Many researchers have tried to explain the behavior of those staking faults created during cooling of silicon crystal in the Czochralski process. It was found that the ring diameter is a sensitive function of the crystal pull rate [1], and temperature gradient at the near the crystal/melt interface in the crystal [2]. The ring radius of OiSF decreases with decreasing growth rate until at the critical value that depends on temperature gradient. A representative OiSF-Ring is shown in Fig. 1 in the MCLT map of an axial cross-section of Czochralski grown silicon crystal after 2 step heat treatments (800°C 4 hours, 1000°C 16 hours).

Inside the OiSF-Ring, high concentration of vacancy-related defects is present. These defects are measured as flow pattern defects (FPDs) or crystal originated particles (COPs). The presence of these and other microdefects has been linked to the failure of devices [3, 4]. Therefore, a few theoretical studies have been attempted to reduce OiSF-Ring diameter. One is the model which is able to predict quantitatively the variation of the OiSF-Ring diameter with simple approach which is based on experimental results [5, 6].

Voronkov [7] has explained microdefect formation in silicon in terms of intrinsic point defect dynamics. Brown *et al.* [8] described the first step of an attempt to the model formation of microdefects by combining atomistic level simulation of the transport and reaction. And Sinno *et al.* [9] described a two-dimensional model for point defect dynamics includes point defect convection by crystal motion, Fickian diffusion, thermo diffusion, and point defect recombination. Sino's description of point defect dynamics is also similar to the model proposed by Voronkov [7] and Brown *et al.* [8]. At least, all of these results offered consistent description of OiSF-Ring dynamics. We also used the same model to calculate the point defect concentration and the OiSF-Ring diameter.

As mentioned before, many researchers have tried to explain the behavior of OiSF-Ring and predict it's location on the wafer by calculation, because the location of OiSF-Ring is a significant data in industry. Especially, we are interested in reducing vacancy rich region without LDP (Large Dislocation Pit) which is generated in interstitial rich region. Furthermore we are concentrating our effort to make COP free wafer has no COP throughout the wafer without any aggregation of interstitial typed defects with one other.

Therefore, we must control the size of V/I boundary (boundary of vacancy rich region and interstitial rich region) to handle the number of vacancy related defects. It is known that V/I boundary and OiSF-Ring are located at almost same position on the wafer although OiSF-Ring is a little bit smaller than V/I boundary. So,

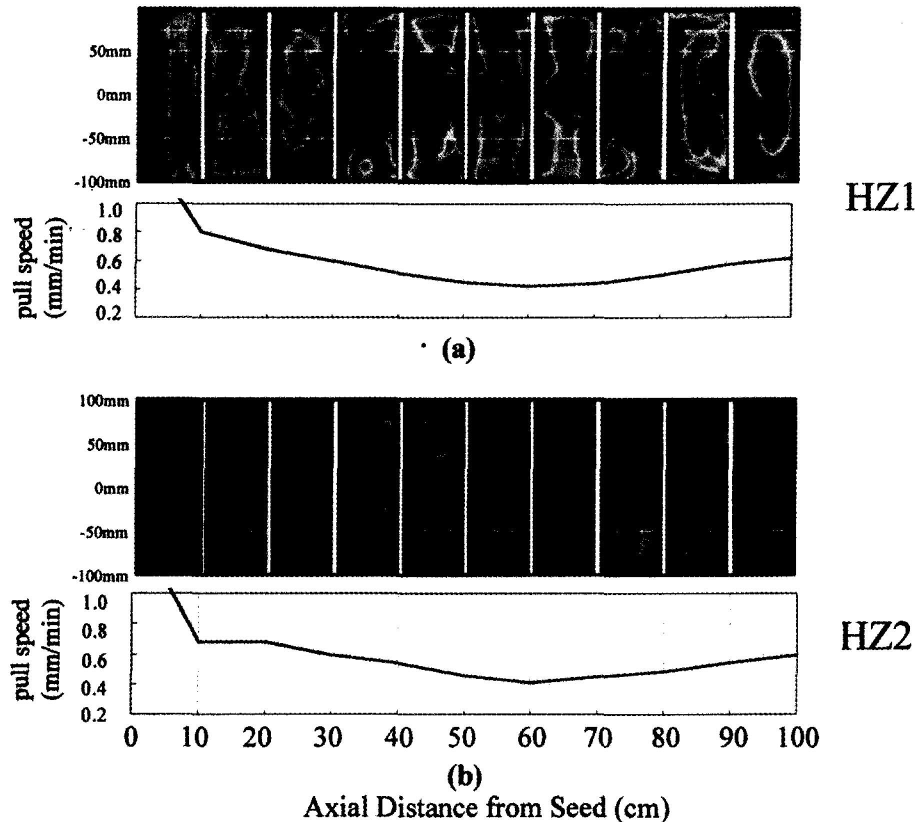

Fig. 1. MCLT map of an axial cross section of 8" Cz-grown silicon crystal and imposed pull speed for the different hot zone configuration HZ1 and HZ2.

if we could calculate OiSF-Ring diameter we could expect the number of vacancy related defects (COP, FPD). In this sense, if we could directly compare numerically simulated OiSF-Ring diameter with real growing data, it would be very useful to develop the advanced wafer in industry undoubtedly. In this work, quantitative agreement was demonstrated for OiSF-Ring diameter between numerical simulation and experiment in an industrial scale Cz silicon crystal growth.

2. Numerical methods

2.1. V/G Fitting

It is known that, OiSF-Ring diameter can be predicted with V/G = 0.138 mm^2/minK [1.2]. Here, V is a pull speed of crystal as an operating variable, and G is an axial temperature gradient at the crystal/melt interface. We have applied this value to our 200 mm CZ growing crystal for two different hot zone configurations. The two systems are denoted as HZ1 and HZ2. In this work G was obtained from numerically simulated temperature distribution using STHAMAS.

STHAMAS developed by Mueller at the University of Erlangen-Nurnberg was used to simulate the temperature distribution in all parts of a crystal puller. It was designed to be used as a tool for the analysis of heat, stress, and mass transfer analysis using multigrid accelerated solver. Different numerical codes for Cz crystal growing are FEMAG and IHTCM which were developed by Dupret and Brown respectively. All three codes are global simulator for Cz crystal growing, namely they predict the temperature distribution in all parts of a crystal puller including crystal, melt, crucible, susceptor, heater, heat shield and insulation. Some differences and common features were discussed in detail by Donberger *et al.* [10].

STHAMAS is a finite volume code based on axially

symmetric geometry and assumed quasi-steady state. In the growth chamber enclosure heat is transferred by radiation which couples the heat flux which is emitted, absorbed and, reflected by solid and liquid surface. All surfaces are included while specular radiation is neglected. And actually, melt flow is 3 dimensional turbulent flow for the industrial scale. However the exact prediction of the melt convection would require the solution of complete set of the Navier-stokes equation with appropriate turbulence model. Up to now this is only possible with super computer. Therefore STHAMAS uses laminar flow model, where the viscosity of liquid silicon is increased by factor of 100 in order to obtain converged solution. This magnifies the viscous force comparing the inertia and buoyancy terms, hence damps the melt flow turbulence.

For the convenience of calculation, we also approximated the melt convection using effective thermal conductivity. Additionally the effective conductivity was locally refined near the crystal/melt interface by analyzing the crystal/melt interface deflection. Figure 2(a) shows the normalized effective conductivity from the center to the crystal radius R near the crystal/melt interface. Figure 2(b) shows the crystal/melt interface deflection when 4 different effective conductivities are imposed. When we used a effective conductivity corresponding case 2, the crystal/melt interface shape was in accordance with experimental data. The case 1 leads more concave interface than experimental data, meanwhile a deep convex interface shapes were calcu-

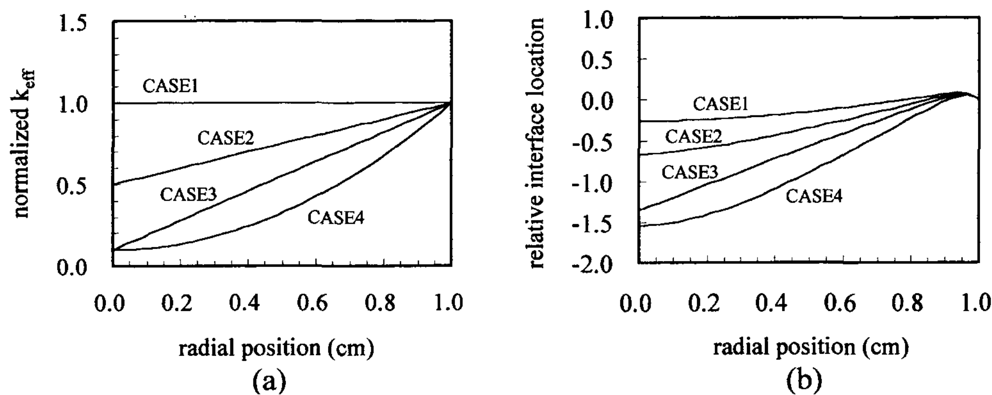

Fig. 2. Relationship between normalized effective thermal conductivity and crystal/melt interface deflection. (a) normalized effective thermal conductivity along the radial direction. (b) Crystal/melt interface deflection when 4 different effective thermal conductivity are imposed.

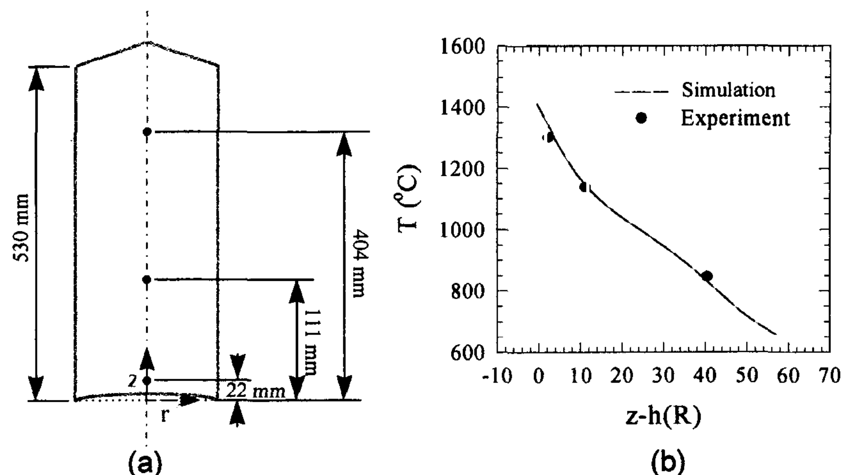

Fig. 3. Temperature measurement experiment using static method. (a) Schematic figure of thermocouple measurement (b) comparison of simulation result and experiment result for 3 points in a Cz grown crystal.

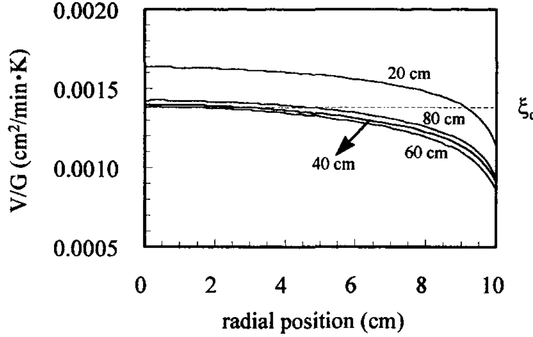

Fig. 4. V/G along the crystal/melt interface for HZ1 configuration according to the crystal length (20 cm, 40 cm, 60 cm, 80 cm).

lated for case 3 and case 4. Therefore we chose case 2 as an effective conductivity for the calculation of temperature distribution.

In order to show validity of predicted temperature distribution using STHAMAS, temperature was measured along the axis of crystal using thermocouples and then compared with computational results. Schematic figure and result are shown in Fig. 3(a) and 3(b). We preferred a static method instead of dynamic method. The 53 cm grown crystal having thermocouples in 3 holes along the axis of crystal was mounted in a Cz silicon puller for 8" crystal. After the steady state was established, temperature was measured by thermocouples. Figure 3(b) represent that measured temperature distribution was quite good agreement with computational result.

Figure 4 shows V/G (r) calculated at the crystal/melt interface from the crystal center to the full radius of 8" crystal with designed pull speed in the fixed hot zone configuration, HZ1, along to the crystal length (20 cm, 40 cm, 60 cm, 80 cm). The straight dotted line represents $(V/G)_{crit} = \xi_c = 0.138\ mm^2/min$ which is the critical condition for the disappearance/appearance of the OiSF-Ring on the wafer surface. The position of OiSF-Ring can be determined at the intersection of V/G curve and ξ_c straight dotted line. OiSF-Ring diameter decreased along the crystal length up to 60 cm. As passed 60 cm, OiSF-Ring diameter increased due to increasing pull speed.

2.2. *Point Defect Dynamics*

OiSF-Ring diameter is also predicted by point defect by dynamics. The model equation to predict the point defect concentration was developed. The continuum balance equations for the transport and interaction of vacancies and interstitials without accounting for the formation of aggregates are written in terms of C_I and C_V (atoms/cm^3).

$$\frac{DC_I}{Dt} = \nabla \cdot \left(D_I \nabla C_I - \frac{C_I D_I H_I^f}{kT^2} \nabla T \right) + k_{IV}[C_I^{eq} C_V^{eq} - C_I C_V], \tag{1}$$

$$\frac{DC_V}{Dt} = \nabla \cdot \left(D_V \nabla C_V - \frac{C_V D_V H_V^f}{kT^2} \nabla T \right) + k_{IV}[C_I^{eq} C_V^{eq} - C_I C_V] \tag{2}$$

Where k_{IV} is the kinetic rate constant for the rate of recombination of vacancies and interstitials and, C_I^{eq} (T) and C_V^{eq} (T) are the equilibrium concentrations of interstitials and vacancies, respectively, at the local temperature T of the crystal. D_I and D_V are the diffusion coefficients and H_I^f and H_V^f are the enthalpies of formation of the point defects and k is the Boltzman constant. Point defect concentrations in the crystal are calculated by using Eqs. (1) and (2) with proper boundary condition. These equations are including bulk convection of point defects due to crystal motion, Fickian diffusion, thermo diffusion, and solid state reactions for self-interstitial and vacancy recombination and generation.

. For the boundary condition, symmetry condition is applied at the axis and no flux condition is applied along the crystal surface. Finally at the crystal/melt interface, the following equilibrium conditions are applied.

$$C_I = C_I^{eq}(T_m) \tag{3}$$

$$C_V = C_V^{eq}(T_m) \tag{4}$$

And relative supersaturation is interpreted in terms of the quantity like as $\Delta \equiv C_I - C_V$ The OiSF is assumed to occur at $\Delta = 0$.

For the modeling of point defect dynamics in silicon, estimating thermo physical parameters and their dependence on temperature are one of the most important problem. The thermo-physical properties of point defect dynamics are as follows;

$$C_I^{eq}(T) = 3.945 \times 10^{26} \exp\left(-\frac{3.943\ eV}{kT}\right) atoms/cm^3, \tag{5}$$

$$D_I(T) = 2.101\times10^{-1}\exp\left(-\frac{0.907\ \mathrm{eV}}{kT}\right)\mathrm{cm}^2/\mathrm{s}, \quad (6)$$

$$C_V^{eq}(T) = 2.675\times10^{23}\exp\left(-\frac{2.848\ \mathrm{eV}}{kT}\right)\mathrm{atoms/cm}^3, \quad (7)$$

$$D_V(T) = 1.000\times10^{-4}\exp\left(-\frac{0.489\ \mathrm{eV}}{kT}\right)\mathrm{cm}^2/\mathrm{s} \quad (8)$$

Although the enthalpies of formation of vacancies and interstitials depend on the temperature, we used the mean value in calculation as $H_I^f = 3.66$ eV and $H_V^f = 2.66$ eV.

The kinetic constant k_{IV} is written as

$$k_{IV}(T) = \frac{4\pi a_r}{\Omega c_s}(D_I + D_V)\exp\left(-\frac{\Delta G_{IV}}{kT}\right). \quad (9)$$

where $a_r = 10$ Å is the capture radius for recombination, W = $1/8a^3$ is the volume occupied by a host atom (a = 5.53 Å for silicon) and $c_s = 5\times10^{22}$ atoms/cm^3 is the atomic density. The free energy barrier for recombination is termed as $\Delta G_{IV} \equiv \Delta H_{IV} - T\Delta S_{IV}$ Unfortunately, there are no precise calculations of these contributions. The enthalpic barrier is used as ΔH_{IV} = 3.173 eV and we use 15 k for ΔS_{IV} The values of the equilibrium, transport and kinetic constants described above can be compared with those from the literature [11, 12]. We believe that our kinetic constants are in the reasonable range comparing others [11].

The finite element method is used for discretization of the complete set of the mathematical model. The concentration fields are represented in expansions of Lagrangian biquadratic basis functions. A mesh is formed of quadrilateral elements which span the computational domains corresponding to the crystal phase. The nonlinear algebraic equations set in linearized by Newton-Raphson method. All unknowns are obtained simultaneously using the Newton iteration scheme. All the contribution to the jacobian matrix are computed in closed form. Numerical nine-point Gaussian quadrature for the volume integrals and three point Gaussian quadrature for the surface integrals are used to calculating the residual and Jacobian matrix. A Frontal solver was imposed to solve the entire set of linear equations and minimize the core memory.

3. Comparison of simulation and experiment for OiSF-Ring

Experimental results for two crystal growth systems, HZ1 and HZ2, are compared to the simulation results by the V/G fitting and the point defect dynamics. Figure 1(a) shows MCLT map of an axial cross-section of Czochralski grown 8" silicon crystal which is grown with decreasing and increasing of pull speed along the crystal length. Figure. 1(b) is same as Fig. 1(a) for the other hot zone configuration HZ2. As the temperature gradient G for HZ1 is larger than for HZ2, the OiSF-Ring diameter decreases more rapidly correspond to the applied pull speed. It can be explained by critical value, $(V/G)_{crit}$ = 0.138 mm^2/minK, which determines the OiSF-Ring diameter. Namely, in the case $(V/G) > (V/G)_{crit}$, vacancy type defects are dominant and $(V/G) < (V/G)_{crit}$, interstitial type defects are dominant. Therefore when the same pull speed is imposed in the different hot zone configurations, larger G leads small OiSF-Ring, otherwise smaller G leads large OiSF-Ring.

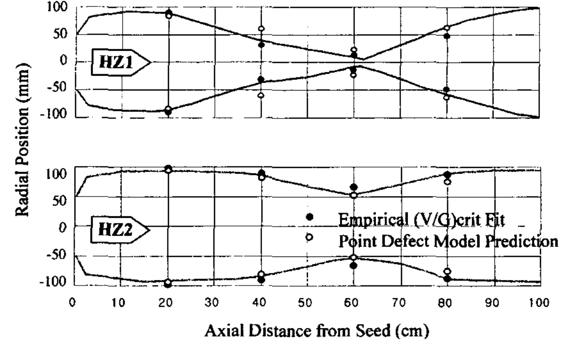

Fig. 5. Comparison of simulation and experiment for OiSF-Ring for HZ1 and HZ2. Solid line present OiSF-Ring obtained by experiment, and circles are by V/G fit, and triangles are by point defect dynamics.

Figure 5(a) and 5(b) represent our experimental results and simulation results which are based on V/G fitting and point defect dynamics. The OiSF-Ring diameters are strongly affected temperature gradient at the crystal/melt interface and pull speed. We found the same tendency from both simulation results. In addition, the position of OiSF-Ring calculated by numerical simulation is very close to the experimental one.

4. Conclusion

The radial position of OiSF-Ring was calculated by (V/G) fitting and point defect dynamics for industrial scale grower with various pull rates. And it was compared with experimental result. In this work, quantitative agreement was obtained between computational

and experimental results.

For the convenience of calculation, we approximated the melt convection using effective thermal conductivity. Additionally the effective thermal conductivity was locally refined near the crystal/melt interface by analyzing the crystal/melt interface deflection.

References

[1] M. Hasebe, Y. Takeoka, S. Shinoyama and S. Natio, Defect Control in Semiconductors, K. Sumino, Ed., Vol. I (Elsevier Science, N.H., 1990) p. 157.
[2] F. Shimura, J. Appl. Phys. 72 (1992) 4.
[3] J. Park and G. Rozgonyi, Solid State Phenomena 47-48 (1996) 327.
[4] S. Winkler, Influence of the Gate Oxide Quality on 4M bit DRAM Device Failures and Reliability 96-13 (1996) 238.
[5] W. von Ammon, E. Dornberger, H. Oelkrug and H. Weidner, J. Crystal Growth 151 (1995) 273.
[6] E. Dornberger and W.V. Ammon, J. crystal Growth 143 (1996) 1648.
[7] V.V. Voronkov, J. Crystal Growth 59 (1992) 625.
[8] R.A. Brown, D. Maroudas and T. Sinno, J. Crystal Growth 137 (1994) 12.
[9] T. Sinno, R.A. Brown, W.V. Ammon and E. Dornberger, J. Electrochem. Soc. 145 (1998) 302.
[10] E. Dornberger and E. Tomzig, A. Seidl, S. Schmitt, H.-J. Leister, Ch. Schmitt, G. Müller, J. Crystal Growth 180 (1997) 461.
[11] R. Habu and A. Tomiura, Jpn. J. Appl. Phys. 35 (1996) 1.
[12] H. Zimmermann and H. Ryssel, Appl. Phys. A 55 (1992) 121.